We are IntechOpen, the world's leading publisher of Open Access books Built by scientists, for scientists

6,900
Open access books available

186,000
International authors and editors

200M
Downloads

Our authors are among the

154
Countries delivered to

TOP 1%
most cited scientists

12.2%
Contributors from top 500 universities

CLARIVATE ANALYTICS

BOOK CITATION INDEX

INDEXED

WEB OF SCIENCE™

Selection of our books indexed in the Book Citation Index
in Web of Science™ Core Collection (BKCI)

Interested in publishing with us?
Contact book.department@intechopen.com

Repair of Turbine Blades Using Cold Spray Technique

Kazuhiro Ogawa and Dowon Seo
Fracture and Reliability Research Institute, Tohoku University
Japan

1. Introduction

Hot section parts of combined cycle gas turbines are susceptible to degradation due to high temperature creep, crack formation by thermal stress, and high temperature oxidation, etc. Thus, regularly repairing or replacing the hot section parts such as gas turbine blades, vanes, and combustion chambers is inevitable. For this purpose, revolutionary and advanced repair technologies for gas turbines have been developed to enhance reliability of the repaired parts and reduce the maintenance cost of the gas turbines. The cold spraying process, which has been studied as not only a new coating technology but also as a process for obtaining a thick deposition layer, is proposed as a potential repairing solution. The process results in little or no oxidation of the spray materials, so the surfaces stay clean, which in turn enables superior bonding. Since the operating temperature is relatively low, the particles do not melt and the shrinkage on cooling is very low. In addition, this technique is based on high velocity (300-1200 m/s) impinging of small solid metallic particle (generally 5-50 μm in diameter) to the substrate. In this spray process, the particles are accelerated by the subsonic gas jet which is usually lower than melting temperature of feedstock. Consequently, this process has solved the problem of thermal spraying, i.e. oxidation and phase transformation. A cold spray system is also simpler than a than low pressure plasma spraying (LPPS) system. Therefore, it has a possibility to apply cold spray technique instead of welding to repair the cracks. In this chapter, it is described that the possibility of applying cold spray technique for repairing the Ni-base turbine blades and its characteristic.

2. Cold spray

Cold spray is a process whereby metallic powder particles are utilized to form a coating or thick deposition by using ultra-high speed impingement upon a substrate (see Fig. 1). The metallic particles range in size from 5 to 50 μm and are accelerated by injection into a high velocity stream of gases. The high velocity gas stream is generated through the expansion of a pressurized, preheated gas through a de Laval (converging-diverging) nozzle. The pressurized gas is expanded to supersonic velocity, with an accompanying decrease in pressure and temperature. The powder particles, initially carried by a separate gas stream, are injected into the nozzle either prior to the throat or downstream of the throat. The particles are then accelerated by main nozzle gas flow and are impacted onto a substrate after exiting the nozzle. Upon impact, the solid particles deform and create a bond with the

substrate. As the process continues, particles continue to impact the substrate and form bonds with the deposited particles, resulting in a uniform coating with very less pores and high bond strength. The term "cold spray" has been used to describe this process due to the relatively low temperatures of the expanded gas stream that exits the nozzle. Cold spray as a coating technique was initially developed in the mid-1980s at the Institute for Theoretical and Applied Mechanics of the Siberian Division of the Russian Academy of Science in Novosibirsk. The Russian scientists successfully deposited a wide range of pure metals, metallic alloys, and composites onto a variety of substrate materials, and they demonstrated that very high coating deposition rates are attainable using the cold spray process.
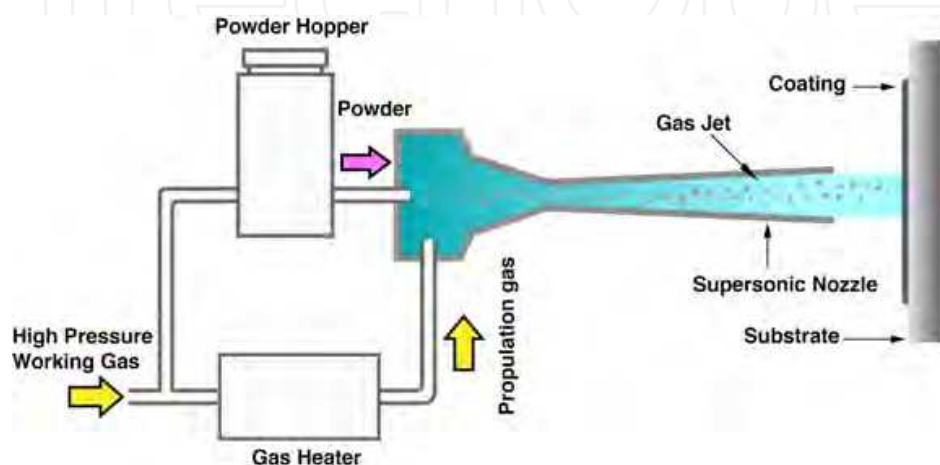

Fig. 1. Schematic illustration of cold spray apparatus

The temperature of the gas stream is always below the melting point of the particulate material during cold spray, and the resultant coating and/or freestanding structure is formed in the solid state. Since adhesion of the metal powder to the substrate, as well as the cohesion of the deposited material, is accomplished in the solid state, the characteristics of the cold spray deposit are quite unique. Because particle oxidation is avoided, cold spray produces coatings that are more durable with better bonding. One of the most deleterious effects of depositing coatings at high temperatures is the residual stress that develops, especially at the substrate-coating interface. These stresses often cause debonding. This problem is compounded when the substrate material is different from the coating material. This problem is minimized when cold spray is used. In addition, interfacial instability due to differing viscosities and the resulting roll-ups and vortices promote interfacial bonding by increasing the interfacial area, giving rise to material mixing at the interface and providing mechanical interlocking between the two materials.

A key concept in cold spray operation is that of critical velocity. The critical velocity for a given powder is the velocity that an individual particle must attain in order to deposit after impact with the substrate. Small particles achieve higher velocities than do larger particles, and since powders contain a mixture of particles of various diameters, some fraction of the powder is deposited while the remainder bounces off. The weight fraction of powder that is deposited divided by total powder used is called the deposition efficiency, and several parameters including gas conditions, particle characteristics, and nozzle geometry, affect particle velocity. And the quality of the cold sprayed coating is affected by not only particle velocity, but also the particle size and size distribution. What seem to be lacking, however, are investigation of influence of particle size distribution. In next section, the influence of the particle size distribution is explained.

2.1 Materials used and spray conditions

A nickel-based superalloy Inconel 738LC (IN738LC) was used in this study. This alloy was solution treated and then subjected to a typical aging treatment. Chemical composition is shown in Table 1 and heat treatment (HT) was applied as following step; first aging at 843°C/24h with air cooling and the second solution treatment at 1121°C/2h with air. Then, the alloy was to form 5.0 mm-thick sheets and vertically sprayed on with a high pressure cold-spray apparatus (PCS-203, Plasma Giken Co., Japan). The thickness of the deposited layer was approximately 800 μm. The powder particles used for cold spraying were prepared from IN738LC (same solution number, gas atomized). The sprayed particles had diameters of less than 25 μm, under 45 μm, and in the range of 25-45 μm. The effect of particle size variation on the strength of the sprayed layer was evaluated. The particle size distribution is shown in Fig. 2. And the spray conditions are displayed in Table 2.

Co	Cr	Mo	W	Al	Ti	Nb	Ta	C	Ni
8.25	15.95	1.7	2.6	3.43	3.42	0.95	1.74	0.11	61.85

Table 1. Chemical compositions of IN738LC (wt.%)
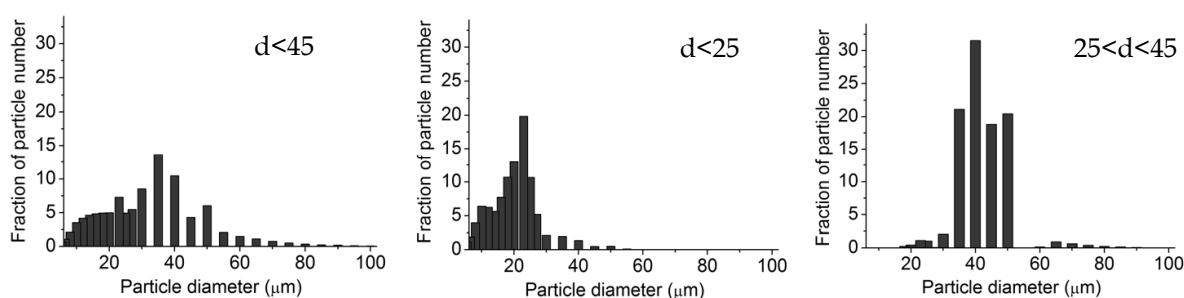
Fig. 2. Particle size distribution using different kinds of powder

Particle size (μm)	Gas type	Temperature (°C)	Pressure (MPa)
d<25	He	600/750/800	2.5/3.5
d<45	He	600/750/800	2.5/3.5
	N_2	650	3.5
25<d<45	He	600	2.5

Table 2. Cold spray conditions

2.2 Microstructures of cold sprayed Ni superalloy coatings

Typical scanning electron microscopy (SEM) images are shown in Fig.3. As shown in these images, it can be made it possible to form thick and dense deposition by cold spray technique. And it is clear that denseness of the cold spray coatings depend on spray conditions. In the case of using 25<d<45 μm powder, in spite of lower gas temperature compared to the others, coating density was high.

Normally, it has been widely accepted that particle velocity prior to impact is one of the most important parameters in cold spraying. It determines whether deposition of a particle or erosion of a substrate occurs on the impact of a spray particle. Generally, there exists critical velocity for materials such that a transition from erosion of the substrate to

deposition of the particle occurs, as previously explained. Only those particles achieving a velocity higher than the critical one can be deposited to produce a coating. The critical velocity (ref. Fig. 4) is associated with properties of the feedstock (Alkimov et al., 1990; Van Steenkiste et al., 1999) and the substrate (Stoltenhoff et al., 2002; Van Steenkiste et al., 1999; Zhang et al., 2003). On the other hand, the particle velocity is related to the physical properties of the driving gas, its pressure and temperature, as well as the nozzle design in the spray gun (Dykhuizen & Smith, 1998; Gilmore et al., 1999; Li & Li, 2004; Van Steenkiste et al., 2002). Ordinarily, higher gas pressure and temperature cause higher particle velocity on cold spraying. Accordingly, by using higher temperature, it can be easy to deposit the particles on the substrate and already deposited particles, and to form dense coatings. However, from the Fig. 3, cold spraying at 600°C has better quality rather than that at 750°C. This means particle size and size distribution are also important for cold sprayed deposition. In the next section, it is described that influence of particle size distribution of used powder focusing on kinetic energy and rebound energy of cold sprayed particles.

d<25 750 °C 2.5 MPa   25<d<45 600 °C 2.5 MPa   d<45 750 °C 2.5 MPa
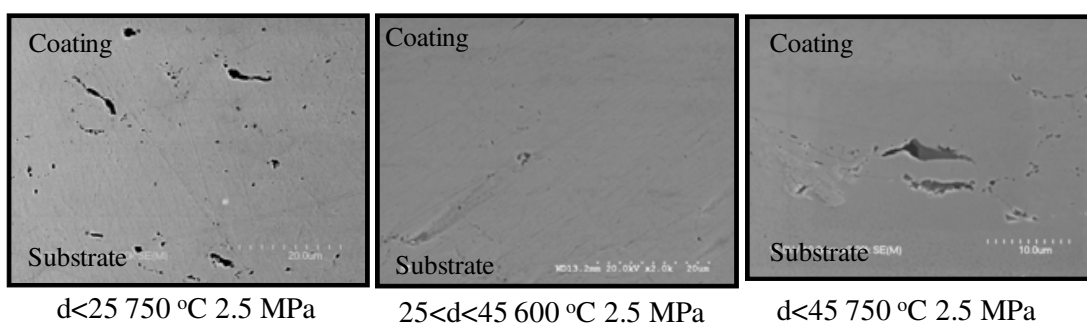
Fig. 3. Examples of typical SEM images of cold sprayed Ni base superalloy coatings
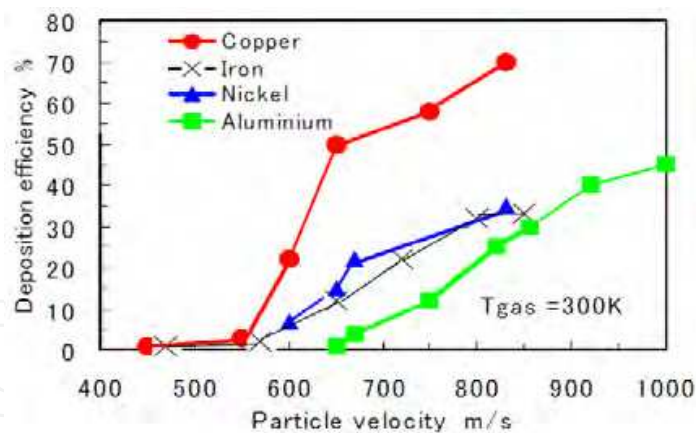

Fig. 4. Critical velocity of cold sprayed depositions

3. Kinetic energy and rebound energy

The cold spraying conditions were optimized by taking into account the particle kinetic energy and the rebound energy for application in repairing gas turbine blades. A high quality cold-sprayed layer is that which has lowest porosity; thus the spraying parameters were optimized to achieve low-porosity layer, which was verified by SEM.

The details on the coating formation mechanism and properties of the cold sprayed layers have not been elucidated thus far. Fukumoto et al. reported that by this technique, high

deposition efficiency was achieved under the conditions of high velocity and high temperature of spraying particles (Fukumoto, 2006; Fukumoto et al., 2007). High velocity particles which have high kinetic energies tend to be more oblate and facilitate deposition. Moreover, erosion behavior can be observed when the particle velocity is low, like grit blasting. Plastic deformation of particles occurs at high kinetic energies of the particles having a high velocity; this plastic deformation induces the formation of a deposited layer. This critical velocity at which deposition begins depends on the mechanical properties of the substrate and the particles, the presence of an oxide layer, and the diameter of the particles. Vlcek et al. have conducted studies on cold spraying of aluminum, copper, and stainless steel on mirror-polished iron and steel to investigate in detail the critical velocities of each metal (Vlcek et al., 2001). In this section, it was suggested that particle impulse (particle mass × velocity) strongly affects deposition efficiency. From the results of the above studies, it can be concluded that the factors that influence the deposition efficiency in cold spraying are: 1) gas temperature, 2) particle mass, and 3) particle velocity. All of these factors depend on the kinetic energy of particles. Therefore, kinetic energy of particles can influence deposition efficiency and influence the strength of the deposited layer.

3.1 Rebound energy during deposition

During cold spraying, all the particles are accelerated by the working gas such as helium and nitrogen. The kinetic energy generated by the working gas induces the deposition. However, part of this kinetic energy is not utilized for the deposition of particles but gets converted to rebound energy. This rebound energy of the particles is calculated by Eq. 1 as follows (Johnson, 1985; Papyrin et al., 2003),

$$R = \frac{1}{2} e_r m_p V_p^2 \tag{1}$$

Here, e_r is the coefficient of rebound, and for spherical particles, its value is expressed as,

$$e_r = 11.47 \left(\frac{\overline{\sigma_Y}}{E^*} \right) \left(\frac{\rho_p V_p^2}{\overline{\sigma_Y}} \right)^{-\frac{1}{4}} \tag{2}$$

Here, $\overline{\sigma_Y}$ and E^* are the yield stress of the particle and the elastic modulus of the substrate, respectively; in this study, the parameters of the alloy IN738LC were determined by conducting proof strength (950 MPa) and indentation tests (201 GPa). ρ_p, V_p, and m_p are the particle density, particle velocity, and particle mass, respectively. In this study, both the particle diameter and mass are sufficiently small. V_p is considered to have the same value as the working-gas flow rate U_g. The U_g is evaluated by the following equation (Eq. 3);

$$U_g = \sqrt{2 \frac{\lambda}{\lambda - 1} R T_i \left[1 - \left(\left(\frac{P_e}{p_i} \right)^{\frac{\lambda - 1}{\lambda}} \right) \right] + U_{gi}^2} \tag{3}$$

Here, U_g and U_{gi} denote the nozzle outlet and inlet rates, respectively; λ and R denote the specific heat ratio and the gas constant, respectively; and P_e and P_i denote the nozzle outlet

and inlet pressures, respectively. The U_g values calculated at different U_{gi} values are summarized in Table 3; during the calculations, P_i was set as atmospheric pressure. Obtained gas flow rates by Eq. 3 are listed in Table 3. From the table, the gas flow rate depends on gas temperature and gas pressure, but is affected by kind of gases in particular.

Gas	Spraying conditions	Gas flow rate at nozzle inlet, U_{gi} (m/s)	Gas flow rate at nozzle outlet, U_g (m/s)
He	800°C, 3.5 MPa	33.04	2910.54
	750°C, 2.5 MPa	23.77	2775.23
	650°C, 3.5 MPa	33.04	2699.48
	600°C, 3.5 MPa	33.04	2625.35
	600°C, 2.5 MPa	23.77	2563.72
N_2	650°C, 3.5 MPa	32.53	1105.50

Table 3. Gas flow rate at nozzle inlet and outlet under different conditions

3.2 Threshold diameter of adhered particle and rebound particle

Fig. 5 shows a schematic illustration of the effect of rebound energy of particles on collision with the substrate. During cold spraying, high velocity particles of various diameters impinge on the substrate. Consequently, the rebound energy of one particle is transferred to the other on collision. Let us that all the kinetic energy of the small particles is converted to adherent energy; Then, if the rebound energy of the coarse particle exceeds the kinetic energy of the small particles, then the rebound energy of coarse particles cause the coarse particles to delaminate into smaller particles, as illustrated Fig. 6. Here, the well-adhered particles are considered to be particles of average diameter. Under this consideration, Eq. 4 was obtained, and the threshold diameter of adherent particle is deduced from Eq. 5, where ρ, σ, and E are parameters characteristic to the particles. Therefore, D_{th} has a unique value.
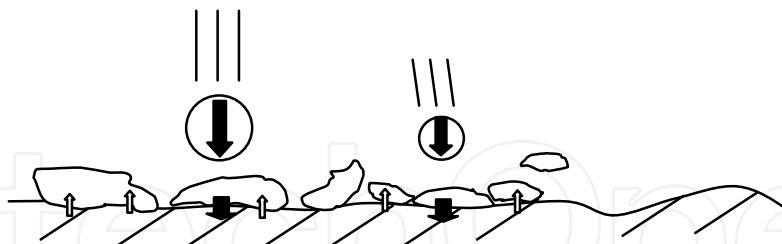
Fig. 5. Schematic illustration of effect of particle rebound energies on substrate
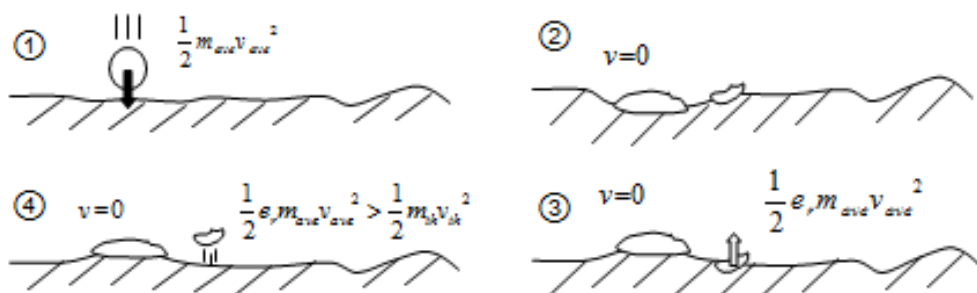
Fig. 6. Schematic illustration of rebound energy to surfaces' particle

$$\frac{1}{2}e_r m_{ave} V_{ave}^2 = \frac{1}{2}m_{th}V_{th}^2 \tag{4}$$

where, $m_{ave} = \frac{4}{3}\pi r_{ave}^3 \rho_{ave}$, $m_{th} = \frac{4}{3}\pi r_{th}^3 \rho_{th}$, and ρ is particle density.

$$D_{th} = 2r_{th} = 2r_{ave}\left[11.47\left(\overline{\frac{\sigma_Y}{E^*}}\right)\left(\frac{\rho_p V_p^2}{\sigma_Y}\right)^{-\frac{1}{4}}\right]^{\frac{1}{3}} \tag{5}$$

If the rebound energy of a coarse particle exceeds the kinetic energy of well adhered particles, then the average-diameter particles can also be delaminated by coarse particle. The diameter of the resultant negative coarse particle can be calculated from Eq. 6.

$$D_{coa} = 2r_{coa} = 2r_{ave}\left[11.47\left(\overline{\frac{\sigma_Y}{E^*}}\right)\left(\frac{\rho_p V_p^2}{\sigma_Y}\right)^{-\frac{1}{4}}\right]^{-\frac{1}{3}} \tag{6}$$

3.3 Equation for optimization of cold spray deposition

The current theoretical principles for cold spray deposition are in Fig. 7. In this figure, it was considered that d<45. The particle distribution result was obtained on the basis of fundamental assumptions. In this result, the kinetic energy used to achieve deposition is that between D_{th} and D_{coa}. Let α represent the number of particle of each diameter; then, the kinetic energy of the deposited particles can be evaluated by Eq. 7. Here, the rebound energy of the coarse particle has a negative effect on the kinetic energy. Therefore, the rebound energy of coarse particle is subtracted from Eq. 7 to give Eq. 8. Thus, $E_{deposit}$ in Eq. 8 represents the effective kinetic energy utilized to achieve deposition. A high $E_{deposit}$ value may imply high deposition efficiency and an improvement in the strength of the adhered layer. Fig. 8 shows the adhesion strength at different spray conditions, as calculated by Eq. 8. The porosity ratios are determined by carrying out SEM observations. The particle diameter and spray conditions are found to affect the quality of the deposited layer. In particular, small particle size can result in the formation of high quality deposited layer.

$$E_{area:M} = \frac{1}{2}*\frac{4}{3}\pi\rho v^2\sum_{r_i=\frac{D_{th}}{2}}^{\frac{D_{coa}}{2}}\alpha_i r_i^3 \tag{7}$$

$$E_{deposit} = \frac{1}{2}*\frac{4}{3}\pi\rho v^2\left(\sum_{r_i=\frac{D_{th}}{2}}^{\frac{D_{coa}}{2}}\alpha_i r_i^3 - \sum_{r_i=\frac{D_{coa}}{2}}^{\infty}\alpha_i r_i^3\right) \tag{8}$$

Optimal particle ranges of each spray condition are listed in Table 4. From the result of Table 4, in the case of condition of d<25, 600°C, He, 2.5 MPa, optimal particle size can be

4.50 to 57.3 μm. The d<25 particle includes less than 4.50 μm particles. These smaller particles can induce formation of porosity or the other defects.
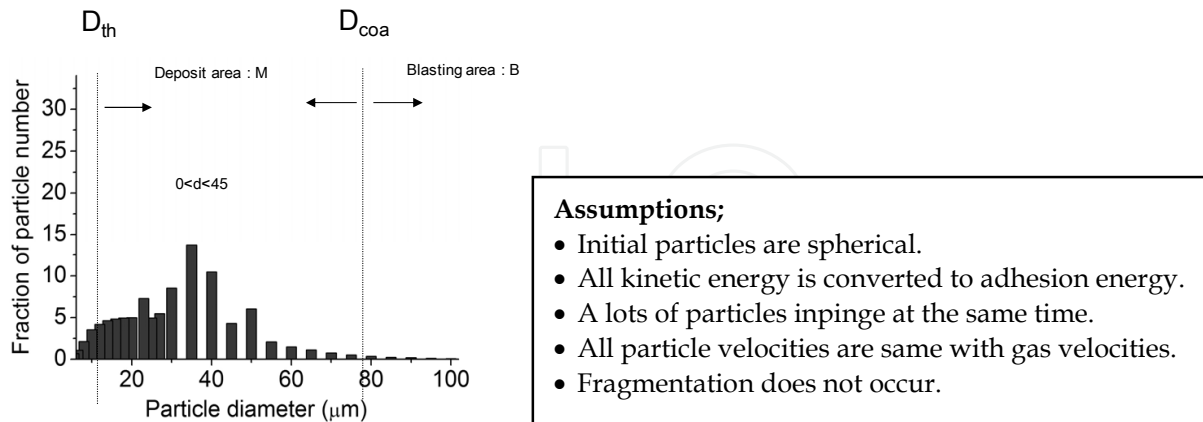

Fig. 7. Particle size distribution and range of particle deposition
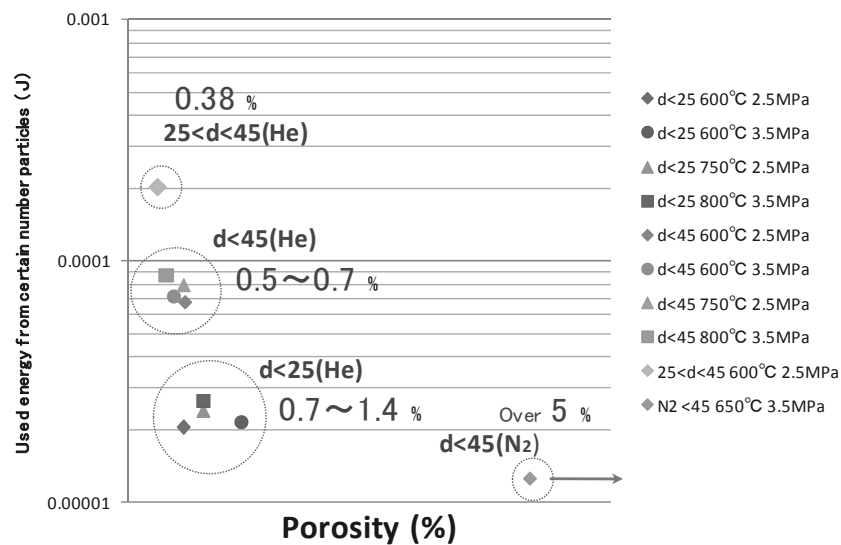
Fig. 8. Evaluation of adhesion strength from Eq. 8

Powder size (μm)	Gas	Temp. (^{o}C)	Pressure (MPa)	D_{th} (μm)	D_{coa} (μm)
d<25	He	600	2.5	4.50	57.3
			3.5	4.47	61.5
		750	2.5	4.51	63.2
		800	3.5	4.47	63.7
d<45	He	600	2.5	6.56	91.0
			3.5	6.49	90.1
		750	2.5	6.58	92.2
		800	3.5	6.74	93.0
	N_2	650	3.5	11.97	123.6
25<d<45	He	600	2.5	10.20	142.7

Table 4. Optimal particle ranges of each spray condition

4. Microstructure and mechanical properties of as-sprayed coatings

Small punch tests were carried out for as-sprayed cold spray coatings as evaluation test of mechanical property. Spraying conditions were particle size of d<25 μm, gas temperature of 650°C, He and N_2 gas with 3.5 MPa. And cross-sectional SEM images of both samples are shown in Fig. 9. The nitrogen gas used coating had many pores, due to lower impinge velocity (ref. Table 3).

Schematic of small punch (SP) test is illustrated in Fig. 10. The samples for SP tests were taken from the cold sprayed deposition. The geometry of the SP specimen was Ø8 mm × 250 μm. The SP specimen was received compressive load by Ø1.0 mm alumina ball. The displacement was measured by Linear Variable Differential Transducer (LVDT). From the SP tests, maximum load and SP energy were evaluated. The schematic of the SP energy is illustrated in Fig. 11. The SP energy was estimated from the area of load-displacement curve. Relationship between applied load and displacement is shown in Fig. 12. And, SP energy is shown in Fig. 13. From Fig. 12, the He gas used specimens are 3 times higher maximum load than that of the N_2 gas used ones. And also, the SP energy of the He gas used specimens was 5 times higher than that of N_2 gas used ones. From these results, mechanical property of the cold sprayed Ni base superalloy coatings depends on coating quality, such as porosity ratio, cohesive force etc.

SEM images of the SP specimens after SP tests are shown in Fig. 14. In the case of the He gas used specimen (see Fig. 14b), radially-propagated cracks were observed. On the other hand, in the case of the N_2 gas used specimen, brittle fracture at the corner of the die was generated. The He gas used specimens, which has higher partcile velocity during spraying, have higher mechnical property than that of N_2 gas used one. However, the maximun load of bulk Ni base superalloys was approximately 1.0 kN in SP tests. This means that the mechnical property of the as-aprayed Ni base superalloy coatings are not enough. It is thought that HT for as-sprayed coatings can be effective for improvement of the mechanical property. And also, it is expected that the HT can control microstructures of cold sprayed coatings. In next section, effects of HT is introduced.



(a) N_2 gas used   (b) He gas used
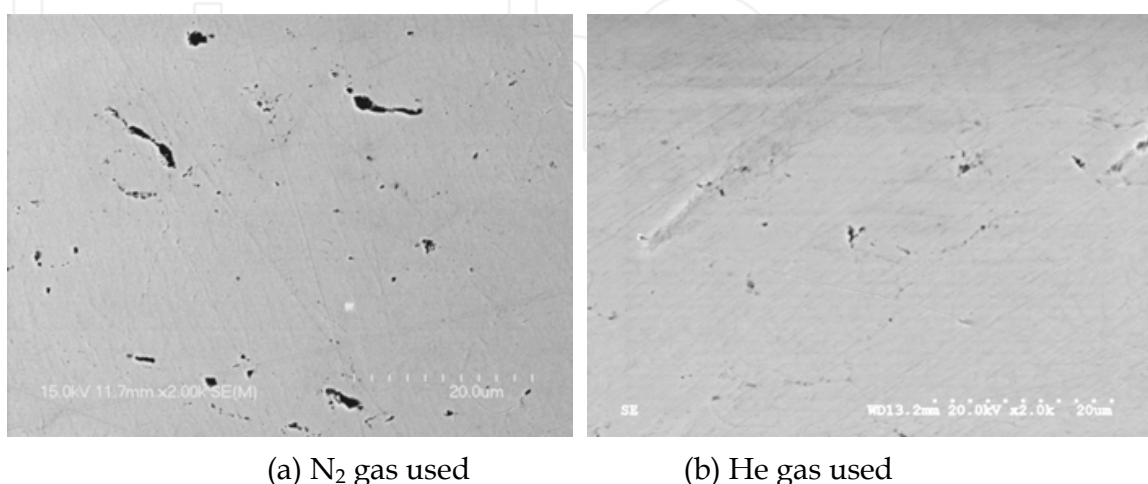
Fig. 9. Typical cross-sectional SEM images of cold sprayed Ni base superalloy coatings
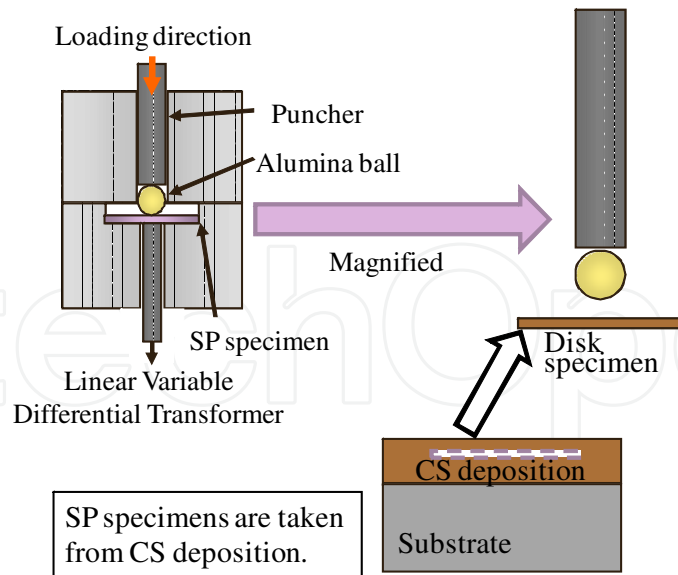
Fig. 10. Schematic illustration of small punch test
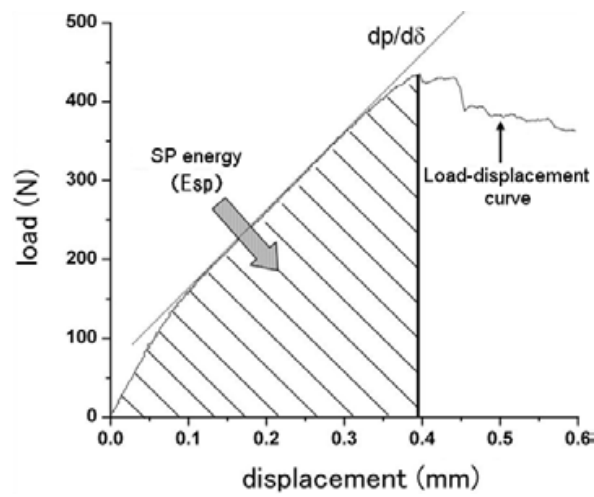

Fig. 11. SP energy
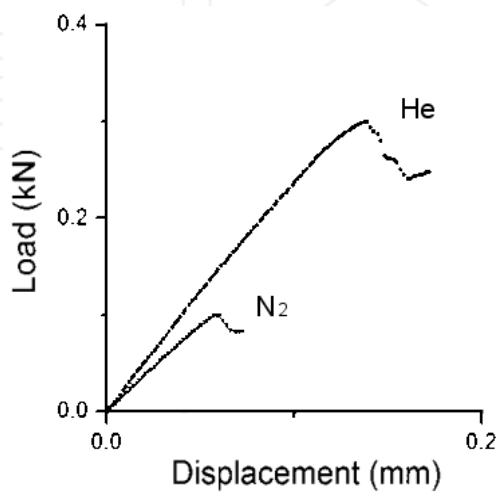
Fig. 12. Results of SP test
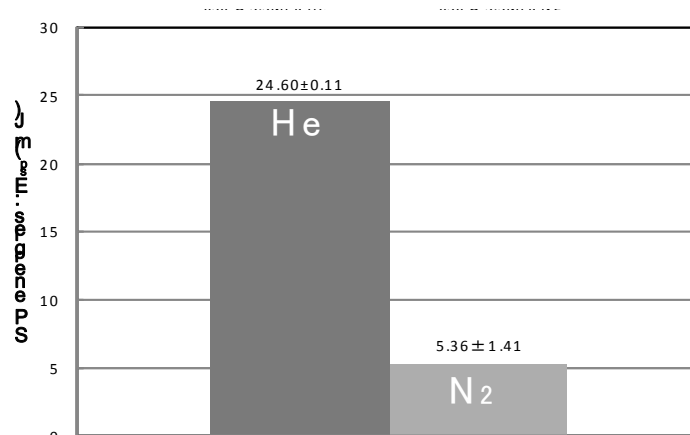
Fig. 13. SP energy of as-sprayed cold spray coatings
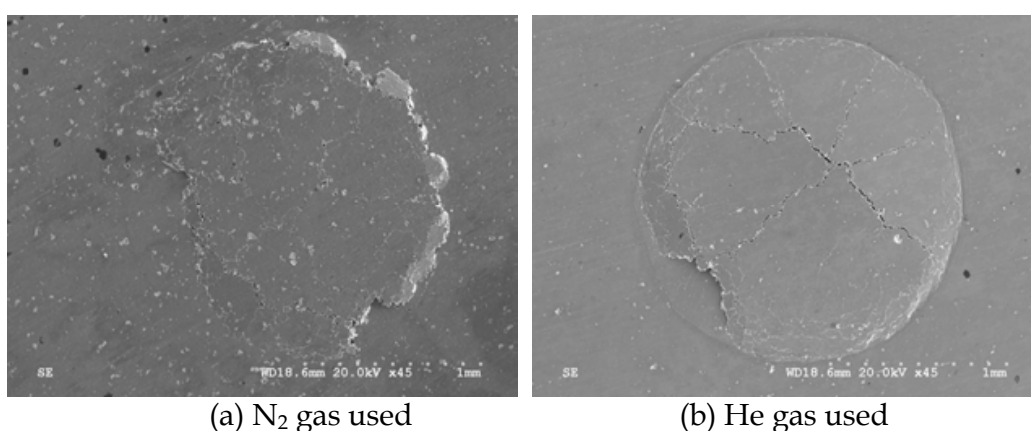
(a) N_2 gas used　　　　　　　　(b) He gas used

Fig. 14. SEM images of the SP specimens after SP tests

5. Post spray heat treatment (PSHT)

For the repair of gas turbine blades, polycrystalline Ni-based superalloy, IN738LC has been studied on the optimization of cold spray process, strength evaluation, and so on. But the mechanical properties of as-sprayed coatings are low compared with bulk materials. In contrast, their properties can be improved by applying standard HT (solution treatment and aging treatment) (Niki, 2009). It was also reported that the mechanical strength, ductility, and adhesion between coating/coating and coating/substrate can be improved by post treatment which causes atomic diffusion between the coating and substrate and the generation of intermetallic compounds (Li et al., 2006; Li et al., 2009; Spencer & Zhang, 2009). Thus many researches relating the post HT are necessary for the cold sprayed coatings. Therefore the following chapter focuses on the metallic structure of the coatings after post HT including the change of γ'-phase before and after HT, precipitation, grain, and so on.

5.1 Microstructure after HT

Fig. 15 shows the sectional micrographs of a) the as-sprayed CS coating and b) one after a standard HT. The existence of pores was confirmed at both samples. From comparing the two micrographs, the improved adhesive interfaces were observed at some location which

revealed that adhesion can be improved by the post HT. Both porosities are shown in Fig. 16 calculated by image processing of cross sectional images. Decrease in porosity is confirmed from the results after HT. Decrease in porosity of yttria-stabilized zirconia coatings after post treatment also was reported (Renteria & Saruhan, 2006; Zhao et al., 2006). It might be resulted from the powder sintering effect by HT over 1000°C. Figs. 17 and 18 show the cross sectional micrographs of the as-sprayed coating and the heat treated coating respectively. In case of as-sprayed coatings, the distorted splats are observed but the grain boundary and intermetallic precipitation of γ′ phases are not observed as shown in Fig. 17b. In case of the coatings applied the post HT, on the other hand, two different grains which have diameter of about 800 nm and 250 nm was observed. It reveals the existence of γ and γ′ phase precipitation. They are irregular in shape, but in case of substrate, two phases are homogeneous in shape as shown in Fig. 19. High temperature strength of Ni-based superalloys such as IN738LC is highly dependent on containing the γ′ phase precipitating. Caron reported that the creep rupture strength of CMSX-2 having the regularly aligned γ′ phase is more higher than one having the irregularly shaped γ′ array (Caron & Khan, 1983) and it was also reported that Alloy143 having the smaller γ′ phase showed higher creep rupture strength at 982°C. From above reasons the appropriate post HT are essential for the cold sprayed coatings including IN738LC to improve their properties.
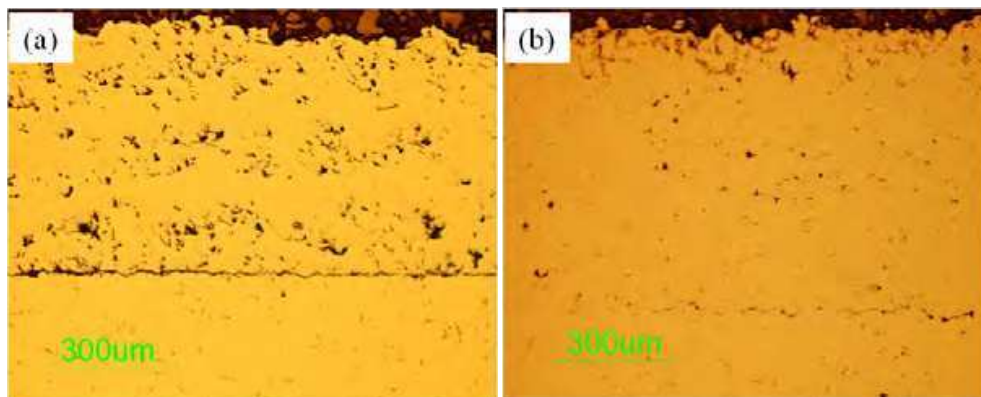
Fig. 15. Cross-sectional micrographs of the CS coatings, a) as-sprayed and b) applied the post HT
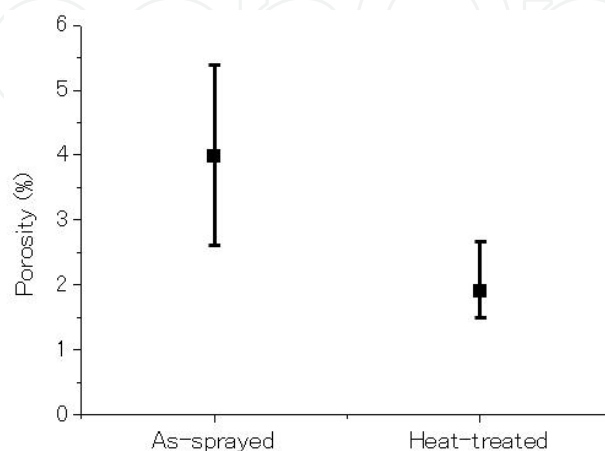
Fig. 16. Porosity measurement before and after HT
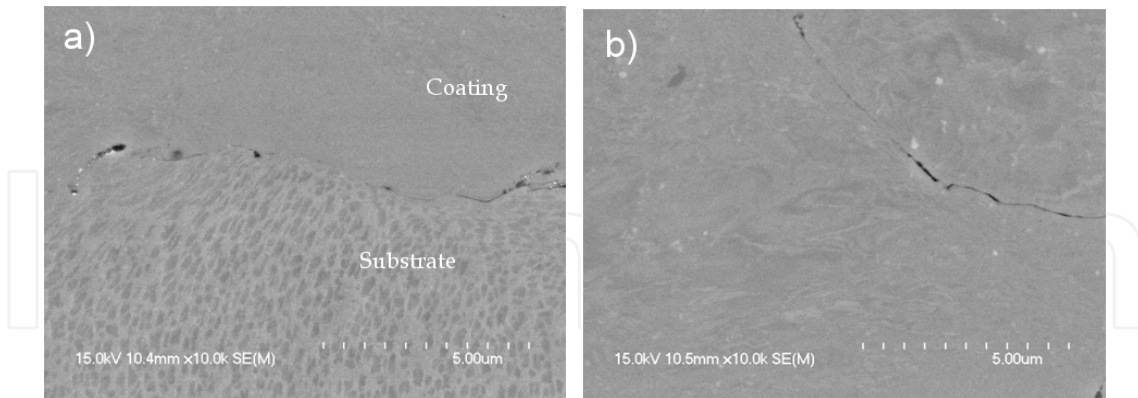
Fig. 17. Cross-sectional micrographs of the as-sprayed CS coatings showing a) the coating/substrate interface and b) near the interface
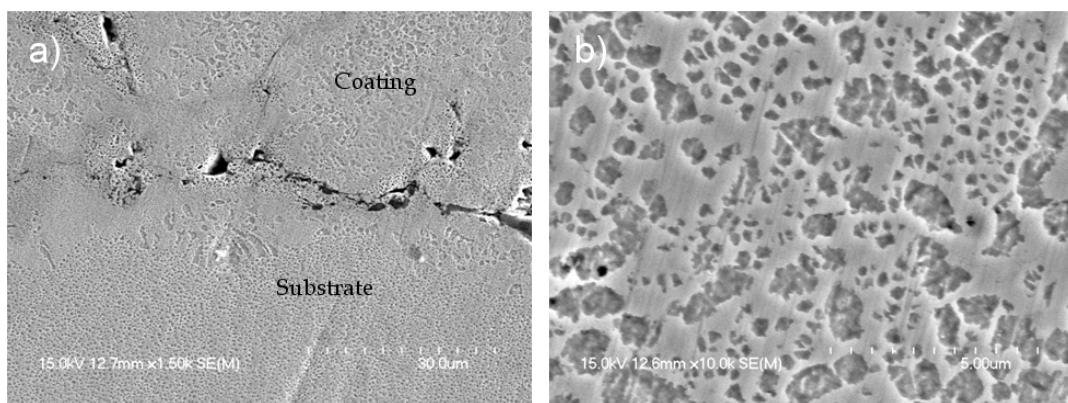

Fig. 18. Cross-sectional micrographs of the CS coating applied the post HT, showing a) the coating/substrate interface and b) the closed view of coating
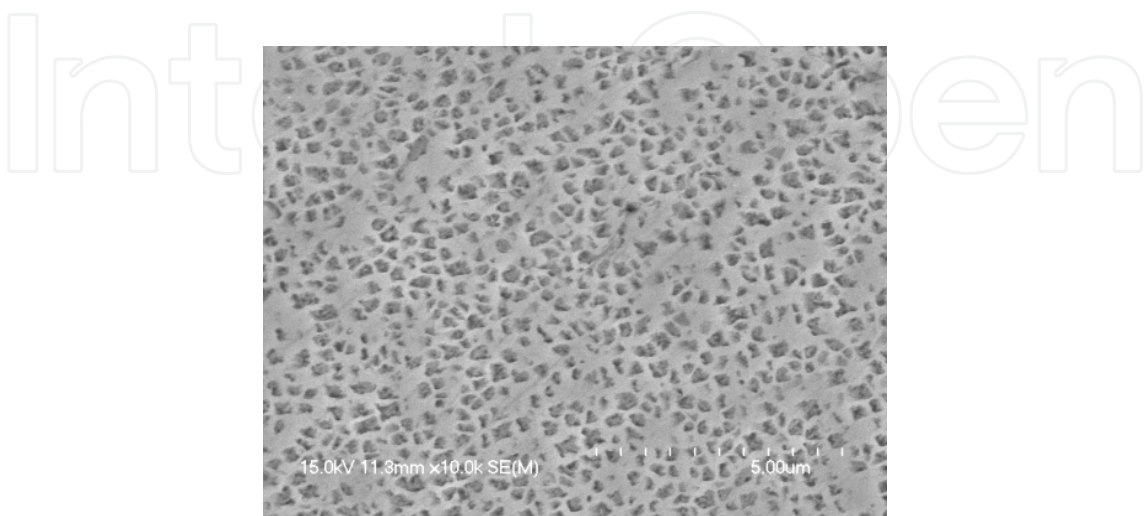

Fig. 19. Micrograph of IN738LC substrate after HT

5.2 Grain structure study via electron back scattering diffraction (EBSD)

From SEM observations, the grains in the as-sprayed coating were not clearly observed. Therefore, in order to observe the detailed structures of the as-sprayed CS coatings before and after HT, the EBSD analysis was carried out which is one of the useful crystallography methods. The EBSD patterns (Kikuchi) were produced when an electron beam incident on the sample surface which represent the crystal orientation. Fig. 20 shows a schematic diagram of the EBSD technique showing the principle of Kikuchi pattern generation and electron beam irradiation. The Kikuchi lines are appeared when the electron beam is reflected via the Bragg reflection angles by the inelastic dispersion of electron within a depth of 50 nm from the sample surface. It is possible to analyze the crystal structure and crystal orientation at the exact point of sample surfaces by electron irradiation. Strain is expected to be introduced inside the coatings during the deposition process. The dislocations might be caused by plastic strain in the coatings. The Kernel Average Misorientation (KAM) can be effective to analyze these dislocation and plastic strain comparing before and after HT.

Image Quality (IQ) map and Inverse Pole Figure (IPF) map representing the distribution of plastic strain were also used together with KAM map. The IQ is displayed in the map as the gray shade which quantified in the sharpness of the diffraction pattern generated from the sample. High value of IQ represents on the map by bright color close to white, and does more clearly where the diffraction pattern is strongly obtained. In general, if the grain boundaries and the distortion are large, or the superposition of patterns from several adjacent crystals, IQ values are decreased and it appears as black lines on the map. IPF is classified by color according to the crystal orientation for each grain. In addition, KAM map is classified by five colors showing the magnitude of plastic strain via the difference in the orientation of each pixel. Blue color indicates the smallest plastic strain and the red color indicates the biggest.

Figs. 21 and 22 shows the IQ map and KAM of the coating and substrate interfaces of the as-sprayed coating and the coating after applied the standard HT. Upper region of each image is the coating and the lower is the substrate. Dark parts on the IQ and IQ + IPF map, reveal that the crystal diffraction corresponding a FCC structure was not detected. In addition, from the EBSD results shown in Fig. 21, most of the diffraction pattern of crystal orientation cannot be seen in case of the as-sprayed coatings. Region that the crystal orientation is not observed is reached over dozens of micrometer from the interface. From the result after HT shown in Fig. 22, the fine grains of 1-20 um in diameter are observed on the coating region. Fig. 23 shows the EBSD analysis of the IN738LC powder prior to the deposition. The grains are clearly observed from the feedstock powder, indicating that the crystal change was occurred after deposition.

The cold sprayed coatings are deposited by large plastic deformation which resulted from the acceleration and collision with the supersonic feedstock powder. In this case, the grain refinement is occurred. Zou et al. reported that the submicron grains were observed after the cold spray deposition with Ni powders via the EBSD analysis (Zou et al., 2009). And Borchers et al. reported that the deformed grains, sub-grains and fine grains are observed in the cold sprayed Ni coating by transmission electron microscopy (TEM) analysis (Borchers et al., 2004). In this study, the amorphous or nano-crystallized grains at the substrate and coating side near the interface are observed which caused from the plastic deformation of feedstock and substrates, and then they recrystallized and grew up to micron size by HT.
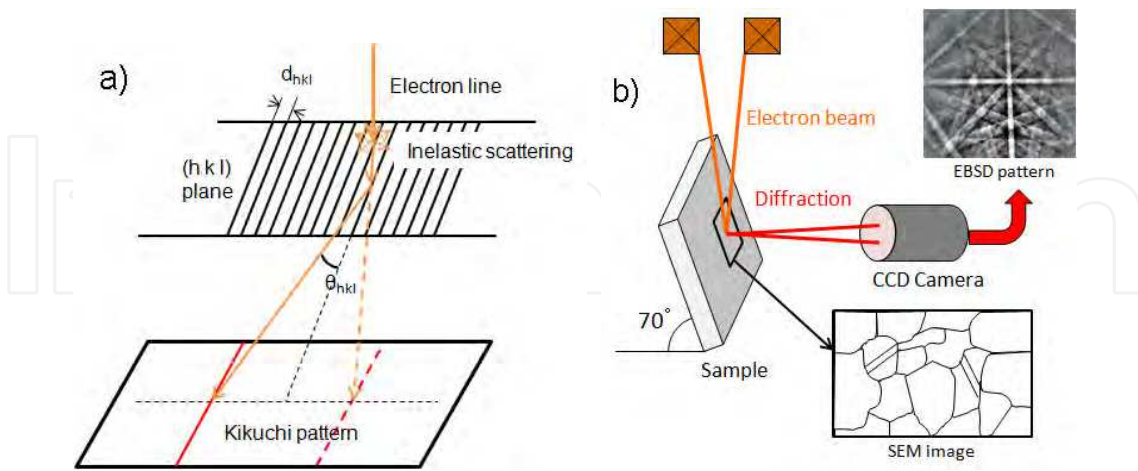
Fig. 20. Schematics presenting a) principle of Kikuchi pattern and b) EBSD technique
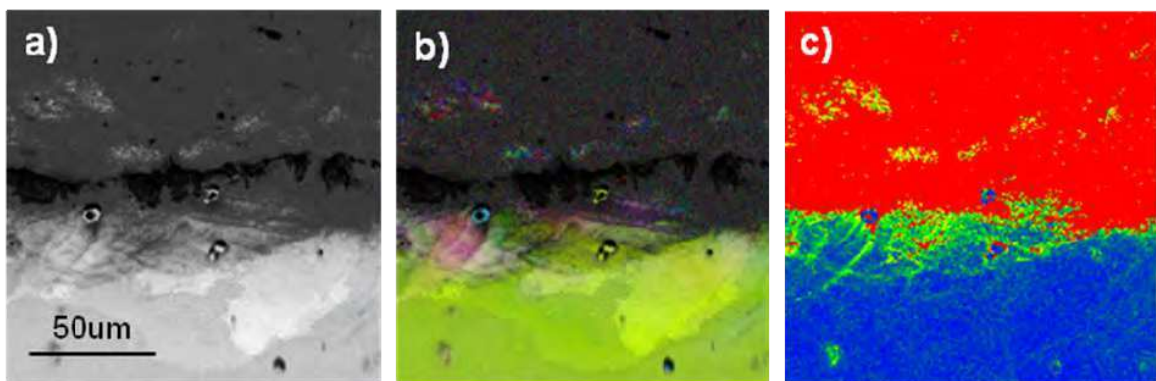
Fig. 21. EBSD analysis of as-sprayed samples; a) IQ map, b) IQ + IPF, and c) KAM map
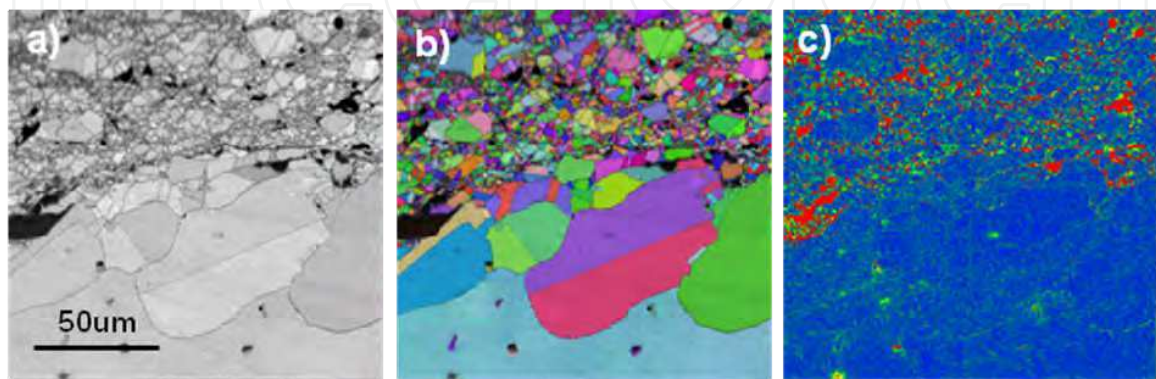
Fig. 22. EBSD analysis of the standard HT sample; a) IQ, b) IQ + IPF, and c) KAM map
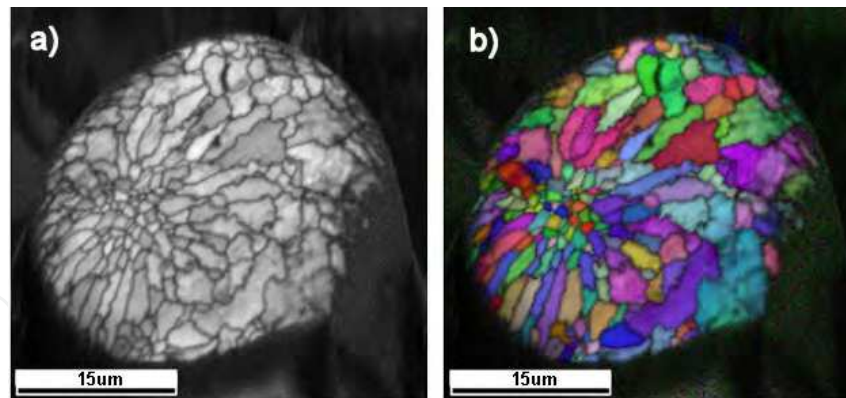
Fig. 23. EBSD analysis of the feedstock powder before spraying; a) IQ and b) IQ + IPF map

5.3 Nanostructure via transmission electron microscopy (TEM) analysis

XRD analysis results described in the preceding paragraph, CS in the deposition of CS μ m depth near the interface and the film was supposed to be because of nano crystals over the substrate, TEM observation was carried out because the nano-sized crystals were observed by XRD analysis. Sampling was made by the focused ion beam (FIB) apparatus, which possesses the coating/substrate interface shown in Fig. 24. The as-sprayed and heat treated samples were prepared for analysis.

Fig. 25 shows the TEM micrographs of the coating/substrate interface of the as-sprayed CS sample. The upper part is the coating area and the lower is substrate, and the white arrows indicate the coating/substrate interface. From this image, the as-sprayed sample is composed of fine crystals from several tens to hundreds of nm order. Fig. 26 shows the crystal orientation analysis in the as-sprayed sample. It was confirmed that the crystal orientation of the six places up to 500 nm in diameter was mixed in disorder at many regions. Especially near the interface, the points of c, d, and e are remarkable. The curved grain boundary was observed from Fig. 25. When the feedstock is attached to the substrate during the deposition by high speed, the severe plastic deformation is occurred in a large scale, and then the curved interfaces are formed from spherical shape of powder as shown in Fig. 27. From the expanded view of the splat boundary shown in Fig. 27, the columnar grain boundaries were observed following a line. Meanwhile, a number of small grains, tens of nm level, have become a gathering at the bottom of the splats. This difference of grain shape may come from the different magnitude and direction of plastic strain during the particle collision. From these results, the schematic diagram of changes in grains of the powder particles and the substrate during deposition can be inferred as Fig. 28. Nano-sized isotropic crystalline was formed at near the bottom surface of the particles as compression direction by the applied strain. In case of side region of coating, the shear strain in the direction parallel to the substrate surface was occurred and the columnar grains deformed along the direction of the strain. From the repeat of particle collision, the deposited coating is composed of columnar crystals and the isotropic nanoscale crystals.

Fig. 29 shows the TEM images at the coating/substrate interface after standard HT. Comparing with the as-sprayed sample in Fig. 25, the growth of large grains can be observed. The coating/substrate interfaces are indicated by white dotted lines and white arrows. As can be seen from this result, the grain was recrystallized and grew in grain size up to micro order, caused by HT. As shown in red and blue lines in the figure, in particularly, the interface to grow to the consolidated form. It can improve the adhesion

strength of the coating/substrate interface by post HT, and such a partial recrystallization at the interface is considered likely to contribute to improve the adhesion of the coating (Zou et al., 2009). In addition, Fig. 30 shows the crystal orientation of four points, a, b, c, and d, around interface in the heat-treated sample. It was confirmed that the grain size of nano-order still remained at point b which close to the surface, even though the points of a, c, and d are single grains. Such nano-grain could be a starting point of coating delamination from the substrate. The post HT with optimal condition are necessary to cover such flaw and then to improve the interface adhesive.
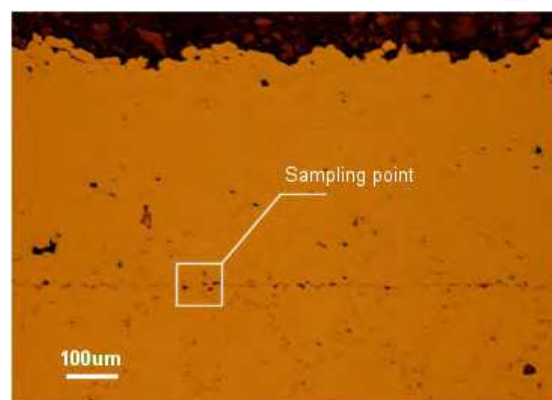
Fig. 24. TEM sampling position
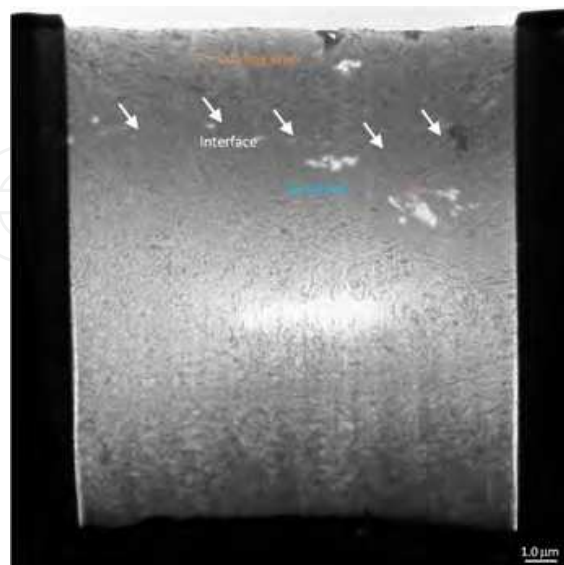
Fig. 25. TEM image at coating/substrate interface of the as-sprayed CS sample
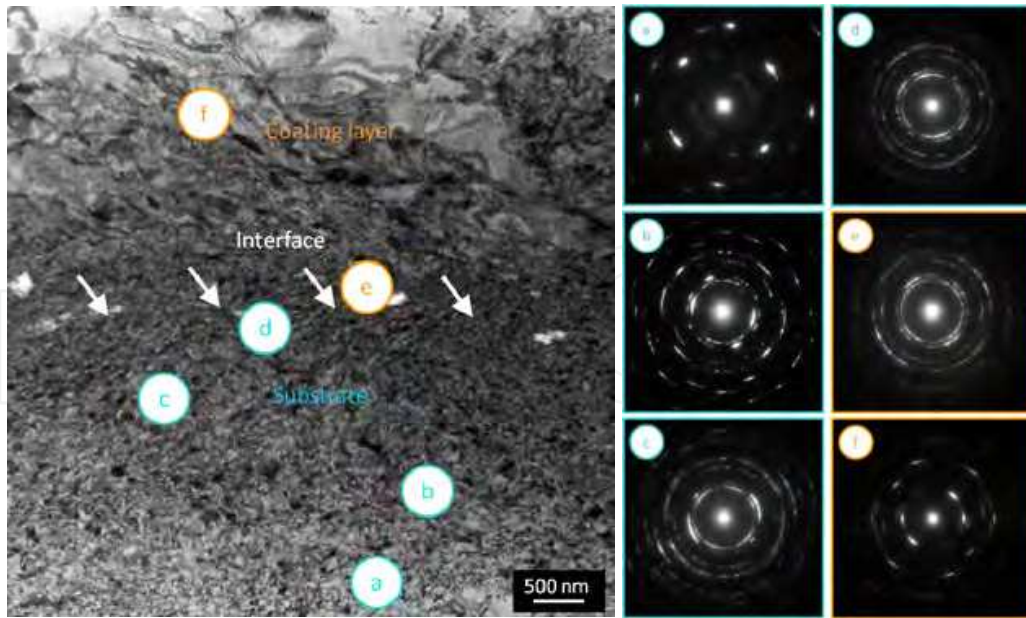
Fig. 26. TEM analysis of crystal orientation at coating/substrate interface of as-sprayed CS sample
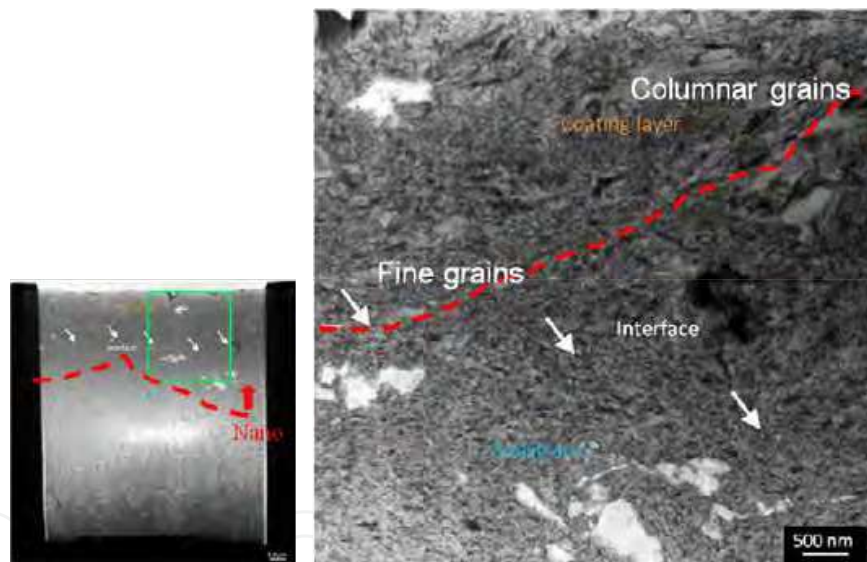
Fig. 27. Magnified image at the coating/substrate interface
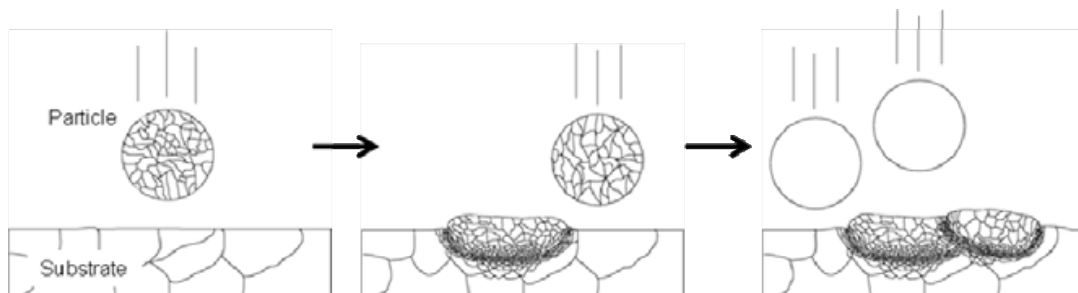
Fig. 28. Schematic of the powder grain changes by cold spraying
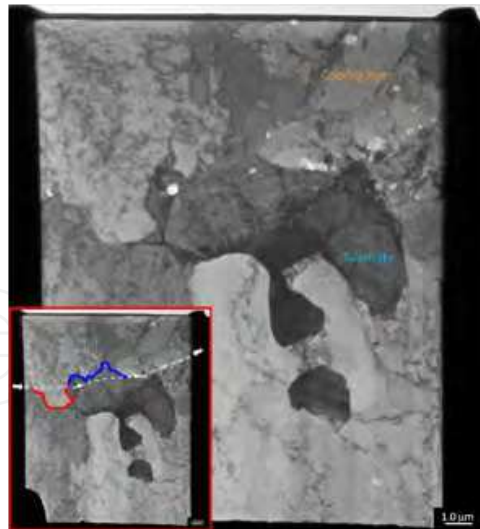
Fig. 29. TEM image at coating/substrate interface after post HT
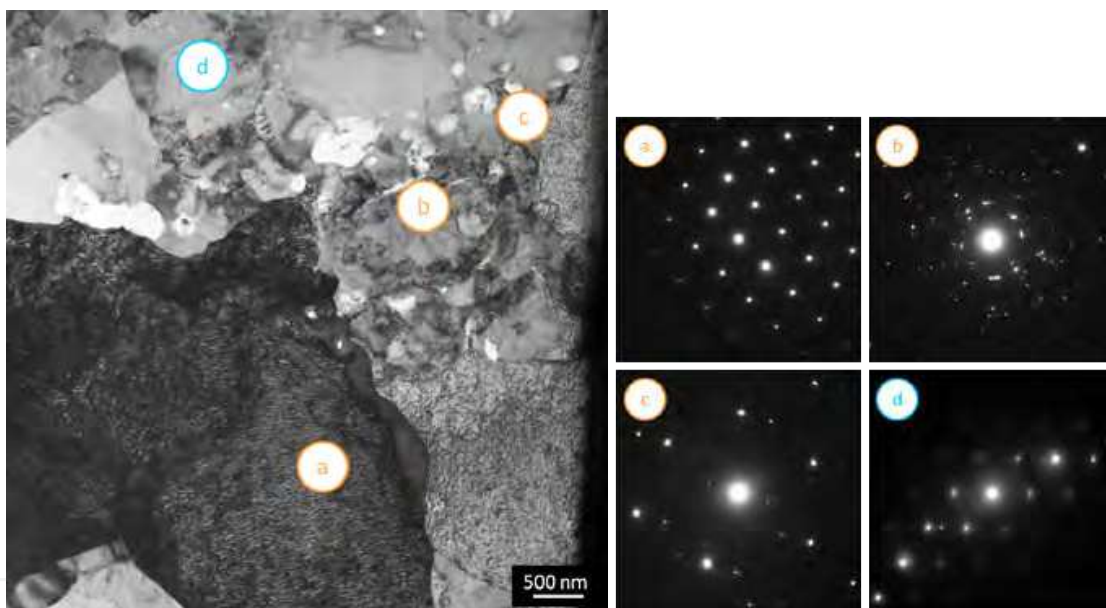

Fig. 30. TEM analysis of crystal orientation at coating/substrate interface after post HT

5.4 High temperature oxidation resistance after post heat treatments

Ni-base superalloys which used as gas turbine blade materials are commonly exposed to high temperature corrosive environment during operation. Among the turbine blade arrays, TBC on the first stage blades is designed to prevent oxidation and corrosion of blade materials from high temperature environment. After long-term use, however, it is frequently reported that the delamination at the interface of TBC system or the weakening of grain boundaries caused by oxidation proceeds from intergranular corrosion in materials, and the cause of crack initiation (Ejaz & Tauqir, 2006; Viswanathan, 2001). As previously mentioned, the grain size in the CS coating is smaller compared to the substrate material (substrate: several hundred microns, CS coating: several microns), and there are also boundaries between the splats. Therefore, it can be considered that oxygen and corrosive

components are easily penetrated to grain boundary compared to the substrate. Therefore In this section, the oxidation resistance of IN738LC CS coatings under high temperature conditions was evaluated together with the effect of post HT on the oxidation resistance property. To evaluate the effect of HT on oxidation properties and to compare, the standard HT (NHT; treated at 1121°C/2h + 843°C/24h) and the high temperature HT (HHT; treated at 1171°C/2h + 843°C/24h) were applied. And the four condition of the exposure time such as 100h, 200h, 500h, and 1000h at temperature of 900°C was applied.

As shown in the Fig. 31, it consisted of double internal oxide layer, i.e., Cr_2O_3 oxide on the coating surface was mainly observed on Ni-base superalloy IN738LC at 900°C, and the scattered γ′ phase of Al_2O_3 also can be categorized into. Thus the evaluation of oxidation characteristics was performed by measurement of the external and inner oxide layer thickness and the average value of them. Figs. 32 and 33 show the thickness of external oxide and inner oxide layer according to the exposure time respectively. And Fig. 34 shows the cross-section images showing the oxide layer of each sample. The surface oxidation was progressed significantly at all samples even though they were exposed to only 500h. It could be resulted from the pore defects in the coatings. For each exposure time and condition, both of the external and internal oxide layers of as-sprayed state were thickest being followed by that of most thick, and following the post HT of NHT and HHT. As a result, each CS sample is considered to be related to grain size in the coating. In case of the external oxide layer, the substrate had the thickest layer than others, but in case of the internal oxide layer, the substrate and the NHT sample show a similar level of thickness.

To investigate what caused these differences, the cross-sectional specimen of each oxide by EDX elemental analysis was performed. From Figs. 35 to 38, they show the EDX analysis for each sample. From the element mapping of each, as noted in previous, the oxide layer on the surface is mainly Cr_2O_3, but the inner consisted of Al_2O_3 and TiO_2. Several elements presented a significant difference was also observed. Comparing the mapping images, Ti element was observed only at the substrate sample. In case of the substrate, Cr_2O_3, TiO_2, and Al_2O_3 were observed as the main oxides. In case of the cold sprayed coating, in contrast, Ti penetrated up to below Al layers. Because the coatings consist of smaller grains compared to the substrate and also the grain boundaries, the oxygen can penetrate and spread easily into the layer, and finally from the oxides.
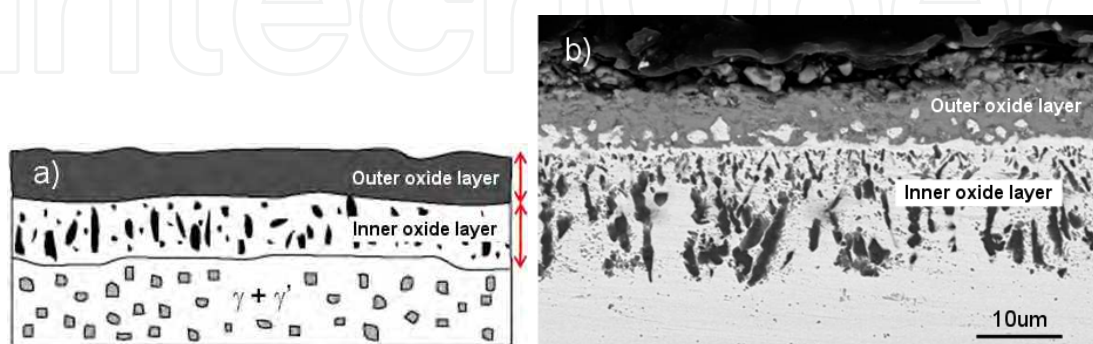

Fig. 31. Oxidation of Ni-based superalloy IN738LC; a) schematic of the double oxide layers and b) SEM image
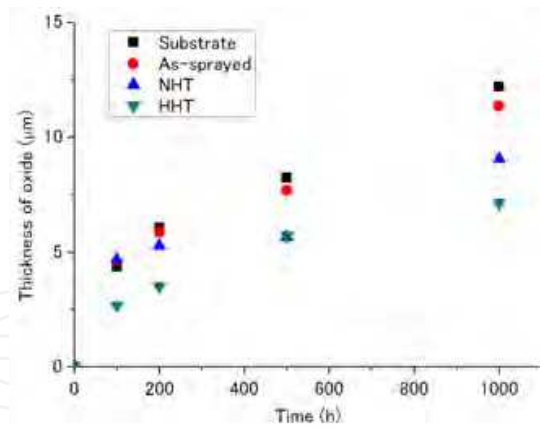
Fig. 32. External oxide thickness of each sample according to exposure time
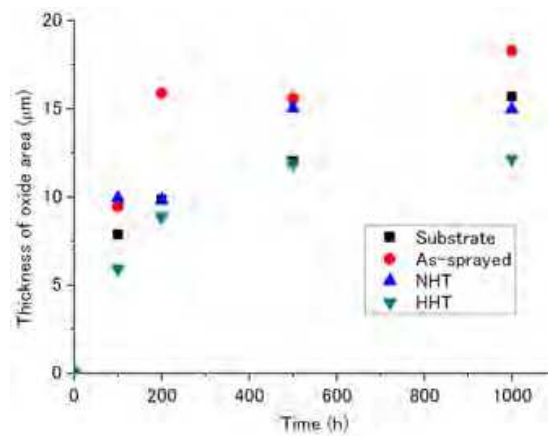

Fig. 33. Inner oxide thickness of each sample according to exposure time
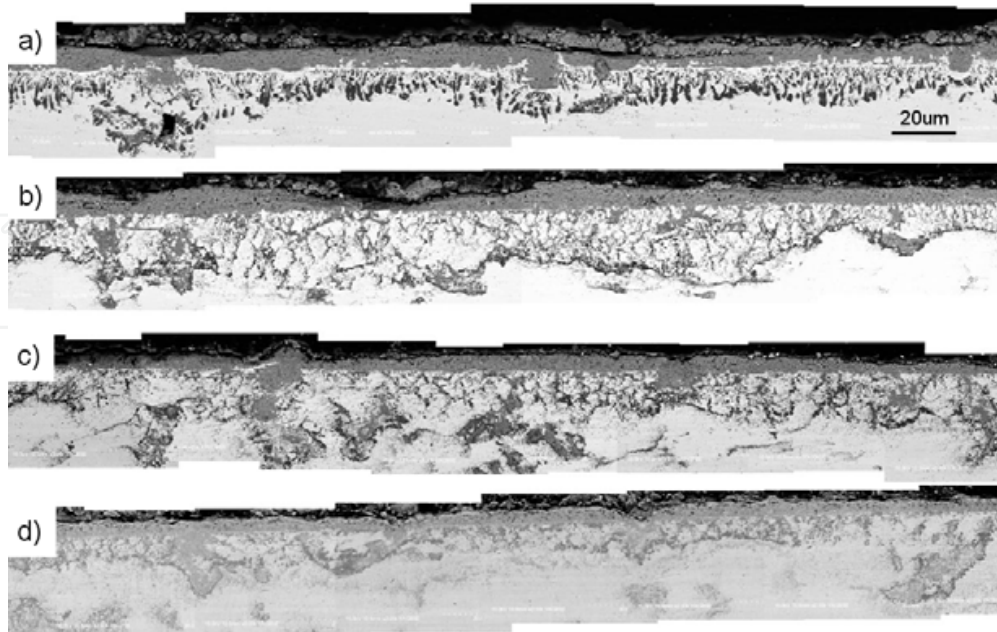
Fig. 34. Cross-sectional images of oxide layer formed at 900°C for 500h; a) substrate, b) as-sprayed, c) NHT, and d) HHT
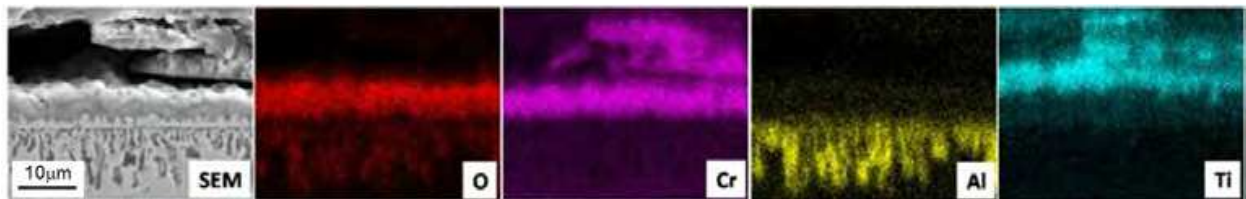
Fig. 35. EDX mapping of the substrate exposed at 900°C for 200h
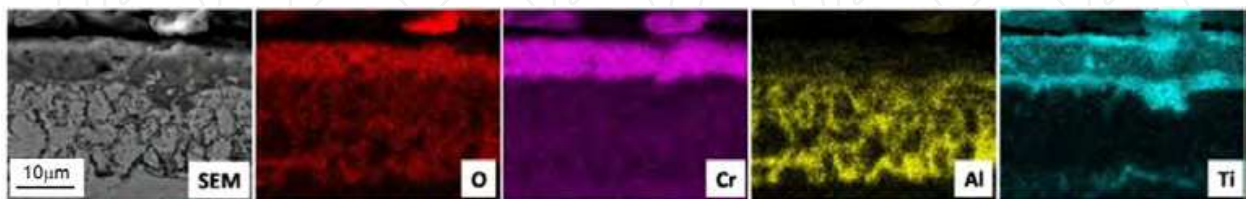
Fig. 36. EDX mapping of the as-sprayed coating exposed at 900°C for 200h
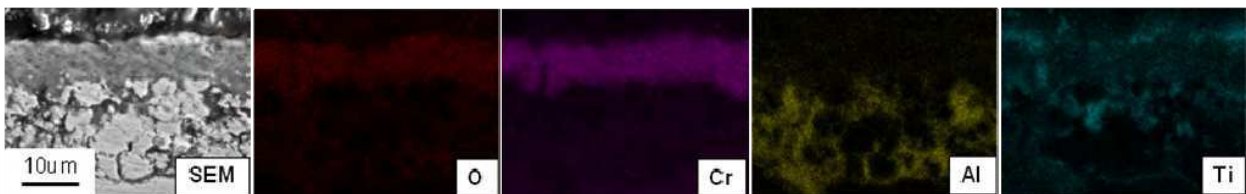

Fig. 37. EDX mapping of the NHT sample exposed at 900°C for 200h
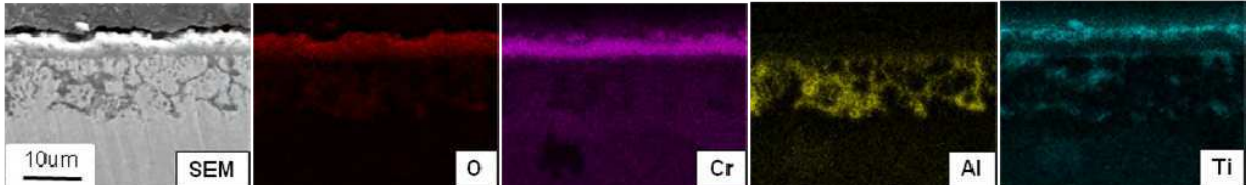
Fig. 38. EDX mapping of the HHT sample exposed at 900°C for 200h

5.5 Small punch tests after post heat treatments

Changes in mechanical properties after HT were evaluated by the maximum load and the absorption energy via the small punch test. Fig. 39 shows the p-δ curves and the SP absorbing impact energy E_{sp} before and after HT respectively. It is clear that the maximum load increased about four times and SP energy also increased about 34 times more after HT. It reveals that the interface adhesion between the coating and the substrate can be significantly improved by applying HT after cold spray deposition of IN738LC. The HT sample in Fig. 39 shows the discontinuous fracture phenomenon with segregation. It may come from the non-homogeneous adhesion between the deposited splats, i.e., some interfaces are improved their adhesive strength via the chemical bonding by the post HT but some part of them cannot bond together due to the gaps between deformed splats. When the cracks progress at the weak region consisted of more gaps, the mechanical load may be released temporarily and result in the segregated load flow.

Figs. 40, 41 and 42 show the SP p-δ curve, SP $dp/d\delta$ curve and SP impact absorbing energy Esp respectively. From Fig. 40, the optimal condition for adhesion layer was to withstand
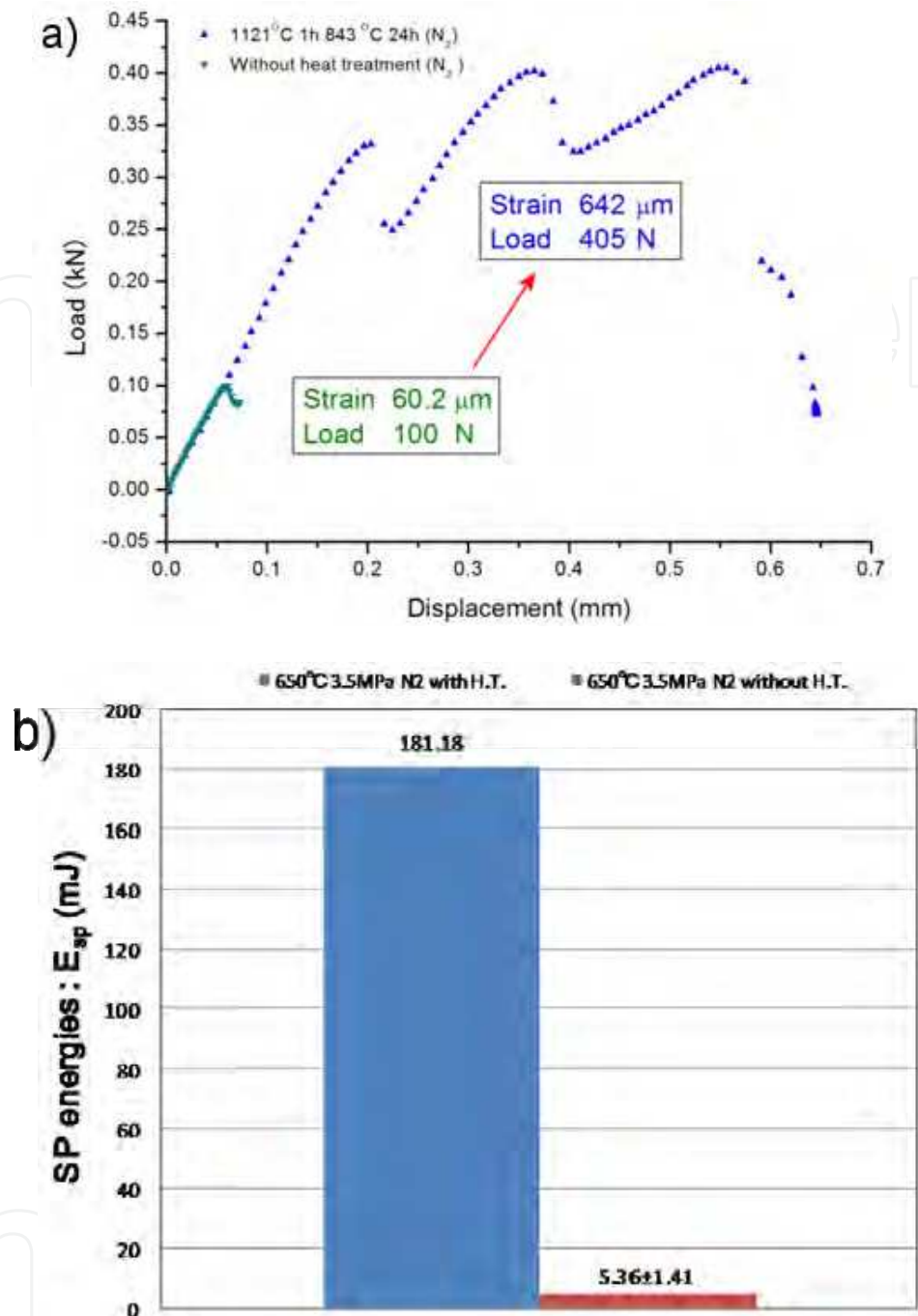
Fig. 39. Comparison of a) p-δ curves and b) SP energy with and without PSHT

about 1.5 times of maximum load after the standard HT. Also refer to Fig. 41, the $dp/d\delta$ value increased about 2-3 times at same condition. From this, even for good adhesion layer, it was found that post spray HT (PSHT) could improve the resistance to deformation or fracture. For a long time thermal aging material which intended for actual use, the maximum load was slightly less compared to the substrate, but SP absorbed energy value of the E_{sp} show about three times of the value of the substrate. Then it became clear that the ductile behavior of the strain to failure increases. Fig. 43 shows the cross-section of SP sample after etching. When the ball was in contact with the substrate/coating interface, it stopped after crack

propagation of about 300 μm. It was found that the crack stopped after propagating into layer shown in figure. It revealed that the interfacial bonding strength among the splats is considered to be sufficiently high after HT. Thus, for repair of the gas turbine blades by cold spray deposition, the PSHT could be admitted the possibility of applying this technique layer from the viewpoint of the better mechanical properties of IN738LC.
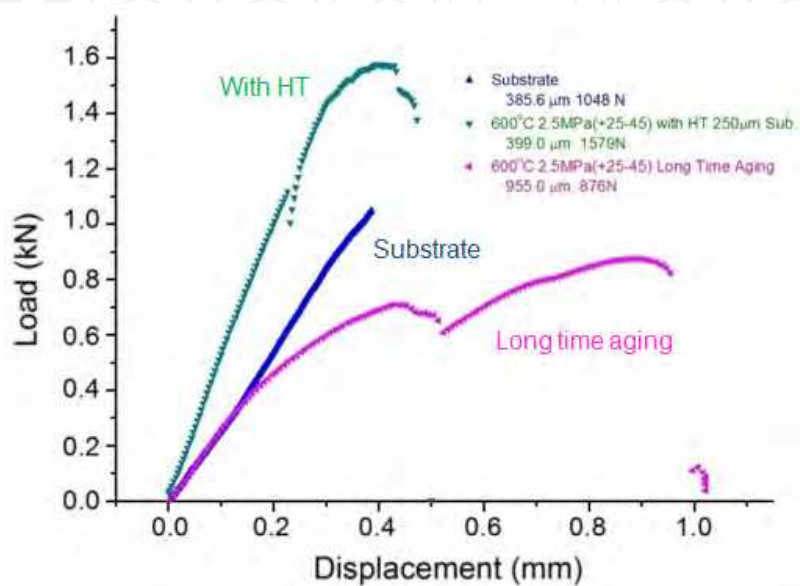
Fig. 40. Comparison of *p-δ* curves with short and long heat treatment
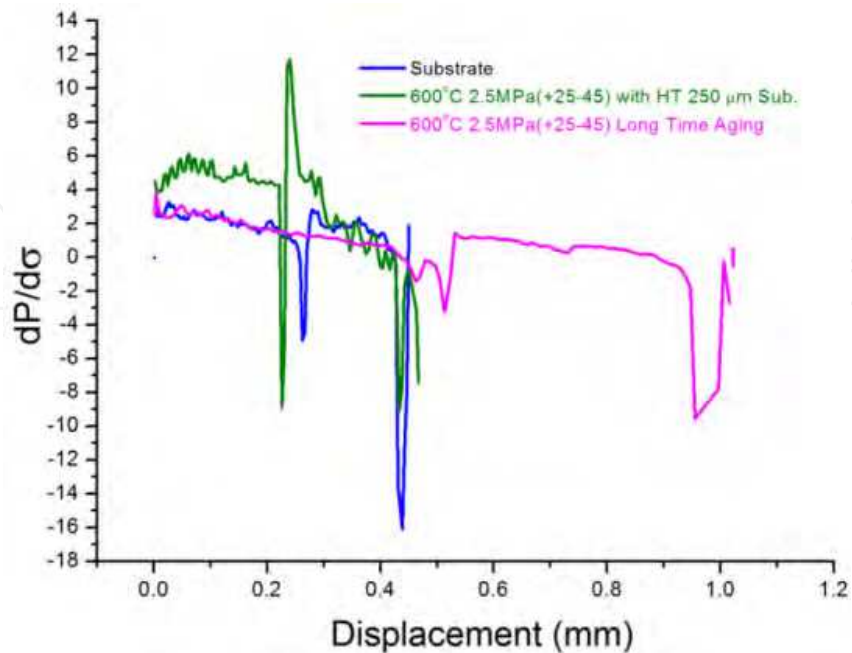
Fig. 41. Derivation of SP *p-δ* curve for each point
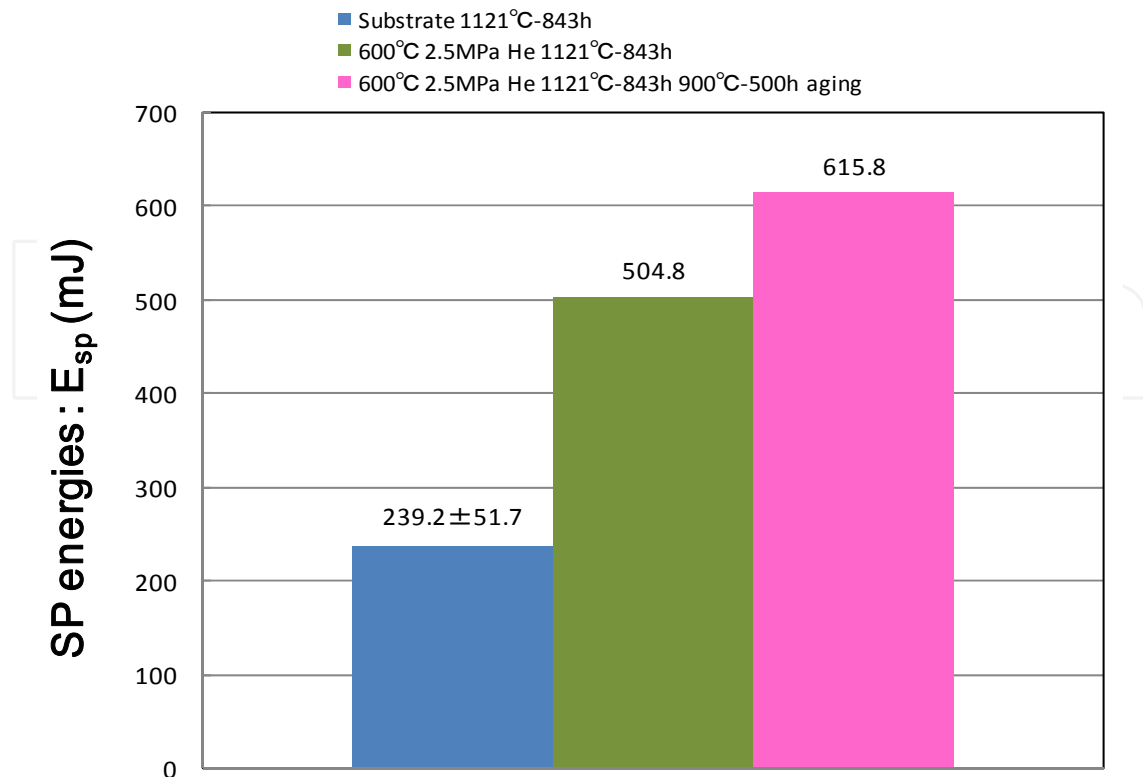
Fig. 42. Comparison of SP energies with short and long heat treatment
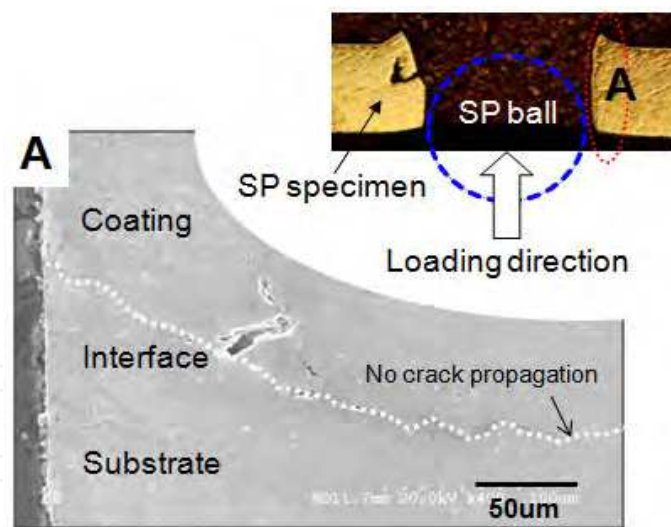
Fig. 43. Cross sectional SEM images of SP specimen

6. Summary

The optimization of cold spraying conditions based on the kinetic energy and rebound energy of the particles was carried out. The particle diameter and spray conditions were found to affect the quality of the diameter deposited layer. In particular, small particle size can effectively improve the quality of the deposited layer. In small punch tests, the He gas used specimens showed are higher maximum load and SP energy than that of the N_2 gas

used ones. However, He gas used coatings are not enough mechanical property compared to bulk Ni base superalloy.

Post heat treatment applied to the cold sprayed coatings was shown to be able to recover their crystalline structure and mechanical properties close to the bulk materials such as substrates. It can improve the adhesion strength of the coating/substrate interface by post heat treatment, and such a partial recrystallization at the interface is considered likely to contribute to improve the adhesion of the coating. It also causes the reduction of pores present inside coatings, the growth of grain size and more γ' phase formation from the as-sprayed state. Particular optimization of the heat treatment conditions is necessary to improve the microstructure and properties.

In each exposure time and condition, both of the external and inside oxide layers of as-sprayed state were most thick, and following the post heat treatment of NHT and HHT. As a result, each CS sample is considered to be related to grain size in the coating. Comparing to the bare substrate sample, the average thickness of the oxide layer of the both NHT and HHT CS samples were thinner at high temperature. This is because the dense grain boundaries near the surface and the formation of Al_2O_3 and TiO_2 in internal layer oxidation.

It revealed that the interfacial bonding strength among the splats is considered to be sufficiently high after heat treatment. Thus, for repair of the gas turbine blades by cold spray deposition, the PSHT could be admitted the possibility of applying this technique layer from the viewpoint of the better mechanical properties of IN738LC.

7. Acknowledgments

8. References

Alkimov, A.P., Kosarev, V.F., & Papyrin, A.N. (1990). A Method of Cold Gas Dynamic Deposition, *Dokl. Akad. Nauk SSSR*, 1990, Vol.318, No.5, (Sep 1990), pp. 1062-1065, ISSN 0002-3264

Borchers, C., Gartner, F., Stoltenhoff, T., & Kreye, H. (2004). Microstructural Bonding Features of Cold Sprayed Face Centered Cubic Metals, *J. Appl. Phys.*, Vol.96, No.8, (Oct 15 2004), pp. 4288-4292, ISSN 0021-8979

Caron, P. & Khan, T. (1983). Improvement of Creep Strength in a Nickel-base Single-crystal Superalloy by Heat Treatment, *Mater. Sci. Eng.*, Vol.61, No.2, (Nov 1983), pp. 174-184, ISSN 0025-5416

Dykhuizen, R.C. & Smith, M.F. (1998). Gas Dynamic Principles of Cold Spray, *J. Therm. Spray Technol.*, Vol.7, No.2, (Jun 1998), pp. 205-212, ISSN 1059-9630

Ejaz, N. & Tauqir, A. (2006). Failure due to Structural Degradation in Turbine Blades, *Eng. Fail. Anal.*, Vol.13, No.3, (Apr 2006), pp. 452-463, ISSN: 1350-6307

Fukumoto, M. (2006). New Trend in Particle Deposition, PD Process and Its Future, *J. Jpn. Weld. Soc.*, Vol.75, No.8, (Dec 2006), pp. 7-11, ISSN 0021-4787

Fukumoto, M., Tanabe, K., Yamada, M., & Yamaguchi, E. (2007). Clarification of Deposition Mechanism of Copper Particle in Cold Spray Process, *Q. J. Jpn. Weld. Soc.*, Vol.25, No.4, (Nov 2007), pp. 537-541, ISSN 0288-4771

Gilmore, D.L., Dykhuizen, R.C., Neiser, R.A., Roemer, T.J., & Smith, M.F. (1999). Particle Velocity and Deposition Efficiency in the Cold Spray Process, *J. Therm. Spray Technol.*, Vol.8, No.4, (Dec 1999), pp. 576-582, ISSN 1059-9630

Johnson, K.L. (1985). *Contact Mechanics*, Cambridge University Press, ISBN 0-521-34796-3, Cambridge, UK

Li, C.J. & Li, W.Y. (2004). Optimization of Spray Conditions in Cold Spraying based on the Numerical Analysis of Particle Velocity, *Trans. Nonferrous Met. Soc. China*, Vol.14, No.2, (Oct 2004), pp. 43-48, ISSN 1003-6326

Li, W.Y., Li, C.J., & Liao, H.L. (2006). Effect of Annealing Treatment on the Microstructure and Properties of Cold-Sprayed Cu Coating, *J. Therm. Spray Technol.*, Vol.15, No.2, (Jun 2006), pp. 206-211, ISSN 1059-9630

Li, W.Y., Zhang, C., Liao, H., & Coddet, C. (2009). Effect of Heat Treatment on Microstructure and Mechanical Properties of Cold Sprayed Ti Coatings with Relatively Large Powder Particles, *J. Coat. Technol. Res.*, Vol.6, No.3, (Sep 2009), pp. 401-406, ISSN 1547-0091

Niki, T. (2009). *Study of Repairing for Degraded Hot Section Parts of Gas Turbines by Cold Gas Dynamic Spraying and its Durability Evaluation*, PhD thesis, Tohoku Univ., Japan, March, 2009

Papyrin, A., Klinkov, S.V., & Kosarev, V.F.; Marple, B.R. & Moreau, C. (2003). Modeling of Particle-Substrate Adhesive Interaction under the Cold Spray Process, *Proceedings of ITSC 2003*, pp. 27-35, ISBN 0-87170-785-3, Orlando, FL, USA, May 5-8, 2003

Renteria, A.F. & Saruhan, B. (2006). Effect of Ageing on Microstructure Changes in EB-PVD Manufactured Standard PYSZ Top Coat of Thermal Barrier Coatings, *J. Eur. Ceram. Soc.*, Vol.26, No.12, (Jun 2006), pp. 2249-2255, ISSN 0955-2219

Sharghi-Moshtaghin, R. & Asgari, S. (2004). The Influence of Thermal Exposure on the γ′ Precipitates Characteristics and Tensile Behavior of Superalloy IN-738LC, *J. Mater. Process. Technol.*, Vol.147, No.3, (Apr 2004), pp. 343-350, ISSN 0924-0136

Spencer, K. & Zhang, M.X. (2009). Heat Treatment of Cold Spray Coatings to Form Protective Intermetallic Layers, *Scr. Mater.*, Vol.61, No.1, (Jul 2009), pp. 44-47, ISSN 1359-6462

Stoltenhoff, T., Voyer, J., & Kreye, H.; Berndt, C.C., Khor, K.A., & Lugscheider, E.F. (2002). Cold Spraying - State of the Art and Applicability, *Proceedings of ITSC 2002*, pp. 366-374, ISBN 3-87155-783-8, Essen, Germany, March 4-6, 2002

Van Steenkiste, T.H., Smith, J.R., Teets, R.E., Moleski, J.J., Gorkiewicz, D.W., Tison, R.P., Marantz, D.R., Kowalsky, K.A., Riggs, W.L., Zajchowski, P.H., Pilsner, B., McCune, R.C., & Barnett, K.J. (1999). Kinetic Spray Coatings, *Surf. Coat. Technol.*, Vol.111, No.1, (Jan 1999), pp. 62-71, ISSN 0257-8972

Van Steenkiste, T.H., Smith, J.R., & Teets, R.E. (2002). Aluminum Coatings via Kinetic Spray with Relatively Large Powder Particles, *Surf. Coat. Technol.*, Vol.154, No.2-3, (May 2002), pp. 237-252, ISSN 0257-8972

Viswanathan, R. (2001). An Investigation of Blade Failures in Combustion Turbines, *Eng. Fail. Anal.*, Vol.8, No.5, (Oct 2001), pp. 493-511, ISSN 1350-6307

Vlcek, J., Huber, H., Voggenreiter, H., Fischer, A., Lugscheider, E., Hallen, H., & Pache, G.; Berndt, C.C., Khor, K.A., & Lugscheider, E.F. (2001). Kinetic Powder Compaction Applying the Cold Spray Process: A Study on Parameters, *Proceedings of ITSC 2001*, pp. 417-422, ISBN 0-87170-737-3, Singapore, May 28-30, 2001

Zhang, D., Shipway, P.H., & McCartney, D.G.; Marple, B.R. & Moreau, C. (2003). Particle-Substrate Interactions in Cold Gas Dynamic Spraying, Proceedings of ITSC 2003, pp. 45-52, ISBN 0-87170-785-3, Orlando, FL, USA, May 5-8, 2003

Zhao, X., Wang, X., & Xiao, P. (2006). Sintering and Failure Behaviour of EB-PVD Thermal Barrier Coating after Isothermal Treatment, *Surf. Coat. Technol.*, Vol.200, No.20-21, (May 2006), pp. 5946-5955, ISSN 0257-8972

Zou, Y., Qin, W., Irissou, E., Legoux, J.G., Yue, S., & Szpunar, J.A. (2009). Dynamic Recrystallization in the Particle/Particle Interfacial Region of Cold-sprayed Nickel Coating: Electron Backscatter Diffraction Characterization, *Scr. Mater.*, Vol.61, No.9, (Nov 2009), pp. 899-902, ISSN 1359-6462
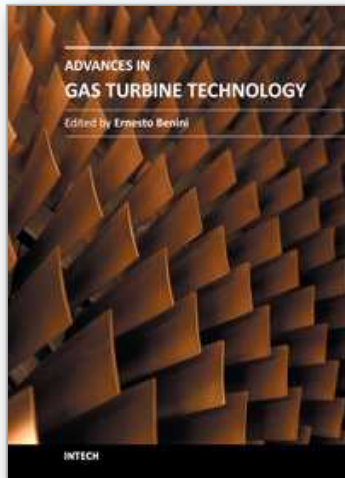
Advances in Gas Turbine Technology

Edited by Dr. Ernesto Benini

Gas turbine engines will still represent a key technology in the next 20-year energy scenarios, either in stand-alone applications or in combination with other power generation equipment. This book intends in fact to provide an updated picture as well as a perspective vision of some of the major improvements that characterize the gas turbine technology in different applications, from marine and aircraft propulsion to industrial and stationary power generation. Therefore, the target audience for it involves design, analyst, materials and maintenance engineers. Also manufacturers, researchers and scientists will benefit from the timely and accurate information provided in this volume. The book is organized into five main sections including 21 chapters overall: (I) Aero and Marine Gas Turbines, (II) Gas Turbine Systems, (III) Heat Transfer, (IV) Combustion and (V) Materials and Fabrication.

How to reference

In order to correctly reference this scholarly work, feel free to copy and paste the following:

INTECH

open science | open minds